2016

Petrogenesis and provenance of distal volcanic tuffs from the Permian–Triassic Karoo Basin, South Africa: A window into a dissected magmatic province

Matthew P. McKay

Matthew A. Coble

Angela M. Hessler

Amy L. Weislogel

Andrea Fildani

Recommended Citation

McKay, Matthew P., Matthew A. Coble, Angela M. Hessler, Amy L. Weislogel, and Andrea Fildani. "Petrogenesis and provenance of distal volcanic tuffs from the Permian–Triassic Karoo Basin, South Africa: A window into a dissected magmatic province." Geosphere 12, no. 1 (2016): 1-14.

Research Paper

THEMED ISSUE: Active Margins in Transition—Magmatism and Tectonics through Time

GEOSPHERE

GEOSPHERE; v. 12, no. 1

doi:10.1130/GES01215.1

6 figures; 1 supplemental file

CORRESPONDENCE: matthewpaulmckay@gmail.com

CITATION: McKay, M.P., Coble, M.A., Hessler, A.M., Weislogel, A.L., and Fildani, A., 2016, Petrogenesis and provenance of distal volcanic tuffs from the Permian–Triassic Karoo Basin, South Africa: A window into a dissected magmatic province: Geosphere, v. 12, no. 1, p. 1–14, doi:10.1130/GES01215.1.

Received 19 June 2015
Revision received 8 October 2015
Accepted 20 November 2015
Published online 7 January 2016

Petrogenesis and provenance of distal volcanic tuffs from the Permian–Triassic Karoo Basin, South Africa: A window into a dissected magmatic province

Matthew P. McKay[1], Matthew A. Coble[2], Angela M. Hessler[3], Amy L. Weislogel[1], and Andrea Fildani[4]

[1]Department of Geology and Geography, West Virginia University, 98 Beechurst Avenue, Morgantown, West Virginia 26505, USA
[2]School of Earth, Energy & Environmental Sciences, Stanford University, Green Earth Sciences Building, 367 Panama Street, Room 89, Stanford, California 94305, USA
[3]Deep Time Institute, 8711 Bluegrass Drive, Austin, Texas 78759, USA
[4]Statoil ASA, 6300 Bridge Point Parkway, #500, Austin, Texas 78730, USA

ABSTRACT

We present zircon rare earth element (REE) compositions integrated with U-Pb ages of zircon and whole-rock geochemistry from 29 volcanic tuffs preserved in the Karoo Supergroup, South Africa, to investigate the history of magmatism in southern Gondwana. Whole-rock compositions suggest a subduction-driven magmatic arc source for early (before 270 Ma) to middle Permian (270–260 Ma) Karoo tuffs. After ca. 265 Ma, the magmatic source of the volcanic deposits transitioned toward intraplate shallow-sourced magmatism. Zircon U-Pb ages and REE chemistry suggest that early to middle Permian magmas were oxidizing, U- and heavy (H) REE–enriched, melts; middle Permian to Triassic zircons record HREE-depleted, more reduced magmatism. Middle Permian to Triassic tuffs contain increasingly large volumes of zircon cargo derived from assimilated crustal material; therefore magmas may have been zircon undersaturated, resulting in less zircon growth and increased inheritance in late Permian to Triassic Gondwanan volcanics. Zircon U-Pb ages and zircon REE chemistry suggest a shift from arc magmatism in the early Permian to extensional magmatism by the late Permian, which may be associated with development of a backarc magmatic system adjacent to western Antarctica that predates known extensional volcanism elsewhere in Gondwana. Opening of the Southern Ocean in the Jurassic–Cretaceous paralleled this extensional feature, which may be related to reactivation of this Permian–Triassic backarc. This study demonstrates the potential of zircon U-Pb age and REE compositions from volcanic tuffs preserved in sedimentary strata to provide a more complete record of magmatism, when the magmatic province has been largely lost to active tectonism.

INTRODUCTION

The magmatic history of igneous provinces is often poorly preserved in the rock record due to rifting of continental crust, orogenic uplift and erosion, and successive intrusion by younger, genetically unrelated magmas along long-lived active margins (Barth et al., 2013). Volcanic tuffs preserved in sedimentary basins, however, have been shown to contain a more complete time-series record of volcanism (Perkins and Nash, 2002) because syntectonic sedimentary basins tend to subside during periods of active magmatism and deformation (DeCelles, 2011). Studies of modern volcanism have shown that the bulk composition of volcanic tuffs varies with distance from the volcanic vent during atmospheric transport (Hinkley et al., 1980; Fruchter et al., 1980; Taylor and Lichte, 1980) through crystal fractionation settling of denser minerals and volcanic glass out of ash clouds during transport (Hinkley et al., 1980). Following eruption and settling of volcanic ash, weathering of chemically unstable glass shards can further alter tuff chemistry and mineralogy (Dahlgren et al., 1993, 1997), further convoluting the petrologic link between the distal deposits and the magmatic source.

Whole-rock trace element geochemical analyses continue to be useful in bridging the link between distal volcanic tuffs and their parental magmas (Tomlinson et al., 2014; Heintz et al., 2015), in particular through the use of immobile trace elements [e.g., Rb, Y, Nb, Zr, and rare earth elements (REEs)] that are less affected by weathering or diagenetic processes in volcanic ashes (Floyd and Winchester, 1978; Hastie et al., 2007). Research into the partitioning of trace elements into zircon (Grimes et al., 2007; Rubatto and Hermann, 2007; Schoene et al., 2012) has proven the potential of zircon chemical analyses to provide insight into deep crustal magmatic processes. Laser ablation–inductively coupled plasma–mass spectrometer (LA-ICP-MS) (Li et al., 2000; Kohn and Corrie, 2011, Kylander-Clark et al., 2013) and secondary ion mass spectrometer (SIMS) analyses (McClelland et al., 2009) techniques now allow for the simultaneous microanalysis of U-Pb isotopic and trace element compositions on single zircon crystals, leading to the development of the relatively new field of petrochronology, which couples radioisotopic ages with trace element geochemical data (Kylander-Clark et al., 2013). Zircon petrochronology has been employed to investigate a wide range of petrologic processes, including the time scales for pluton construction (Barboni et al., 2013; Chelle-Michou et al., 2014), crustal melting (Barth et al., 2013; Gordon et al., 2013), high-grade metamorphic processes (Rubatto, 2002; Hiess et al., 2015), volcanic tuff deposits,

and tephrochronology (e.g., Schmitt et al., 2010; Harvey, 2014). In this study we use whole-rock major [SiO_2, TiO_2, Al_2O_3, FeO (total), MnO, MgO, CaO, Na_2O, K_2O, P_2O_5] and trace element (Ni, Cr, Sc, V, Ba, Rb, Sr, Zr, Y, Nb, Ga, Cu, Zn, Pb, La, Ce, Th, Nd, U, Cs) compositions combined with zircon U-Pb isotopic and REE compositions from distal volcanic tuffs in the Karoo Supergroup of South Africa to investigate the evolution of Permian–Triassic magmatism along the margin of southern Gondwana. Although whole-rock geochemistry data from Permian Karoo tuffs are comparable to those of known transitional magmatism in South America, zircon U-Pb ages and REE compositions in Karoo tuffs record evidence of a transition from hydrous, more evolved magmatism in the early to middle Permian to drier, more primitive magmatism in the middle to late Permian. The timing of this magmatic shift and zircon geochemistry are not compatible with known South American volcanics and so a reevaluation of the volcanic source is required. We explore the implications of the zircon U-Pb and REE data when coupled with whole-rock data from volcanic tuffs to characterize a volcanic system that has been largely lost to active tectonism.

GEOLOGIC BACKGROUND

The Carboniferous–Triassic Karoo Supergroup of South Africa preserves distal volcanic deposits that were erupted from a continental magmatic system along the southern margin of Gondwana (Veevers et al., 1994; Bangert et al., 1999; Pankhurst et al., 2006; Fildani et al., 2007; Fig. 1). The Karoo tuffs have widely been suggested to be sourced by the same magmatism responsible for eruption of ignimbrite sequences interbedded with clastic continental strata in central South America within the Permian Choiyoi Group and Puesto Viejo Formation (Bangert et al., 1999; Cole, 1992; López-Gamundi and Rossello, 1998; Rocha-Campos et al., 2011). Choiyoi Group magmatism can be characterized as two distinct igneous suites generated during different phases of southern Gondwanan tectonic history. The early to middle Permian lower Choiyoi Group contains rocks with a volcanic arc affinity characterized by low Zr (<200 ppm), Nb (<15 ppm), and Y (<80 ppm) with generally higher Sr/Y (>40) compositions, sourced from active subduction along the southern Gondwana margin (Pankhurst et al., 2006; Kleiman and Japas, 2009). In contrast, the middle to late Permian upper Choiyoi Group volcanic rocks indicate a post-orogenic magmatic source and contain elevated Zr (100–700 ppm), Nb (10–35 ppm), and Y (70–90 ppm), and low Sr/Y (<40) (Kleiman and Salvarredi, 2001; Kleiman and Japas, 2009). Following a period of magmatic quiescence (251–240 Ma), the Triassic Puesto Viejo volcanic rocks were erupted during a phase of continental extension and rifting (Ramos and Kay, 1991; Kleiman and Japas, 2009).

Despite this strong historic correlation of Karoo Supergroup tuffs with South American volcanic centers, the distance between the southern Karoo Basin and known volcanism along the Gondwanan margin would have been >1000 km (Bangert et al., 1999; Lanci et al., 2013). The grain size of Karoo tuffs, including casts of pyroclastic grains, suggests a more proximal volcanic source, possibly as close as 100–300 km from the basin (McLachlan and Jonker, 1990; Bangert et al., 1999). Closer candidates for alternate volcanic sources have not been identified, primarily because large portions of the crust where more proximal volcanic source may have existed have been tectonically destroyed or buried through rifting and opening of the Atlantic and Indian Oceans. Portions of Antarctica, the Antarctic Peninsula, and other

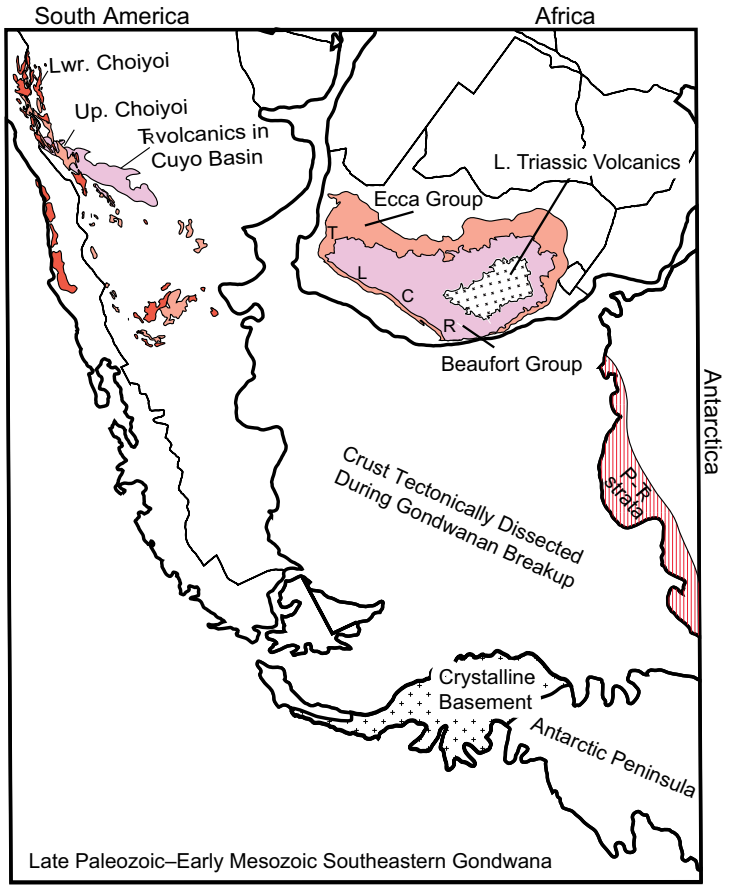

Figure 1. Simplified geologic map of southwestern Gondwana (López-Gamundi and Rossello, 1998) shows the approximate locations of the Karoo Basin, Permian–Triassic volcanic suites in South America (Choiyoi and Puesto Viejo), western Antarctic volcanogenic sediments (Elliott et al., 2015a, 2015b), and Antarctic Peninsula igneous suites (Riley et al., 2012). Lwr., L.—lower; Up.—upper. This study looks to compare the volcanic tuffs from the Karoo Basin to potential igneous sources in South America and Antarctica to evaluate volcanic provenance and the implications for Gondwanan tectonism. Note the large area between Africa and the active margin dissected during opening of the Atlantic and Southern Oceans. The approximate locations of Karoo Basin depocenters are shown: denoted by T—Tanqua, L—Laingsburg, C—central Basin, R—Ripon.

terranes (i.e., Thurston Island and Marie Byrd Land) are thought to have been adjacent to these missing crustal blocks (Lawver et al., 1992). Therefore, the Karoo tuffs may have been sourced by volcanic systems located in the dissected Gondwanan crust adjacent to Antarctic terranes. The Antarctic terranes record Cambrian through Jurassic magmatism and metamorphism (Millar et al., 2002). Permian–Triassic granitoids are located in crystalline basement terranes (Riley et al., 2012), and ignimbrites are present in Permian–Triassic strata in Antarctic sedimentary basins. Locally sourced volcanic tuffs in the late Permian Polarstar Formation, similar to age-correlative tuffs in the Karoo Basin and South America, contain abundant recycled zircon grains (Elliot et al., 2014), suggesting a history characterized by long-lived magmatism and crustal recycling processes.

Absolute stratigraphic age controls (Fig. 2) have been difficult to obtain for the middle Permian–Middle Triassic volcanic rocks in southern Gondwanan (Domeier et al., 2011; Ottone et al., 2014; McKay et al., 2015). U-Pb SHRIMP (sensitive high-resolution ion microprobe) studies of the Choiyoi and Puesto Viejo volcanics have shown that recycled and/or inherited zircon grains are predominant in late Permian–Early Triassic tuffs; a few zircon crystallization ages interpreted to be syneruptive make interpretation of the age of eruption and deposition difficult (Spalletti et al., 2008; Rocha-Campos et al., 2006; Domeier et al., 2011). Ages for volcanic rocks in South America have been obtained through a combination of U-Pb zircon and $^{40}Ar/^{39}Ar$ ages (Spalletti et al., 2008; Rocha-Campos et al., 2006; Domeier et al., 2011, Ottone et al., 2014). Volcanic deposits from the lower Choiyoi Group yield U-Pb zircon ages that range from 282 to 265 Ma (Rocha-Campos et al., 2011). Upper Choiyoi Group rocks yield U-Pb zircon ages that range from 265 to 251 Ma (Rocha-Campos et al., 2011), and are within error of $^{40}Ar/^{39}Ar$ plateau ages of 260 Ma (biotite) and 256 Ma (K-spar) from correlative rocks (Domeier et al., 2011). Puesto Viejo volcanic rocks display $^{40}Ar/^{39}Ar$ amphibole and potassium feldspar ages that are younger than U-Pb zircon from the same samples (Domeier et al., 2011). While the lower Puesto Viejo Group rocks typically yield ca. 265 Ma U-Pb zircon ages, $^{40}Ar/^{39}Ar$ plateau ages range from 235 Ma (K-spar) to 254 Ma (biotite), with a number of samples producing ca. 240 Ma plateau ages in amphibole and K-spar (Domeier et al., 2011). These ages are significantly younger than U-Pb zircon ages from the Puesto Viejo Group, suggesting that zircon crystallization predates eruption and cooling by >10 m.y.

Zircon U-Pb geochronology of Karoo Supergroup tuffs also revealed a scarcity of zircon with syneruptive ages in Permian–Triassic volcanic deposits (McKay et al., 2015). This lack of syneruptive zircon led to a number of contradictory age results for the Karoo Supergroup (Fildani et al., 2007, 2009; Lanci et al., 2013; Rubidge et al., 2013; McKay et al., 2015). The age paradox resolved in South American volcanic suites is likely linked to long-term magmatic zircon recycling (Domeier et al., 2011; Ottone et al., 2014) and similar zircon recycling may be the cause of the age controversy in the Karoo Supergroup strata (McKay et al., 2015). Based on U-Pb zircon age populations and stratigraphic position, tuffs in the Ecca Group are coeval with the upper Choiyoi Group volcanic rocks (265–250 Ma), and tuffs in the Beaufort Group correlate to the Triassic (younger than 240 Ma) Puesto Viejo Group. This correlation, however, is based entirely on geochronology, and no geochemical evidence has been presented to link the South African and South American volcanic deposits.

WHOLE-ROCK GEOCHEMISTRY

Methods

Whole-rock geochemistry from 41 volcanic tuff samples from the Karoo Basin were determined by X-ray fluorescence (XRF) and ICP-MS at the Washington State University GeoAnalytical Lab. Samples were collected from continuous tuff horizons that showed no signs of reworking (cross-bedding or possible unconformable surfaces were not observed; however, grading was present) within mud intervals in the encasing strata to avoid reworked material. Major element oxide [SiO_2, TiO_2, Al_2O_3, FeO (total), MnO, MgO, CaO, Na_2O, K_2O, P_2O_5] and trace element compositions (Ni, Cr, Sc, V, Ba, Rb, Sr, Zr, Y, Nb, Ga, Cu, Zn, Pb, La, Ce, Th, Nd, U, Cs), along with volatile content (loss on ignition, LOI) were collected using XRF methods described by Johnson et al. (1999). For ICP-MS analyses, samples were analyzed for trace and REE concentrations (La, Ce, Pr, Nd, Sm, Eu, Gd, Tb, Dy, Ho, Er, Tm, Yb, Lu, Ba, Th, Nb, Y, Hf, Ta, U, Pb, Rb, Cs, Sr, Sc, Zr) (methods as described by Lichte et al., 1987; Jarvis, 1988; Jenner et al., 1990; Longerich et al., 1990). Elemental concentrations were determined by both XRF and ICP-MS for Sc, Ba, Rb, Sr, Zr, Y, Nb, La, Ce, Th, Nd, U, Cs; 90% of the XRF measured concentrations are within ±10% of the ICP-MS results (~70% of XRF results are within ±5% of ICP-MS values), suggesting good agreement between both analytical techniques. We analyzed 4 samples 2–3 times to assess instrumental drift and reproducibility; multiple analyses showed no significant instrumental bias or analytical variability.

Results

Major element concentrations for 41 volcanic tuffs (Table 1 in the Supplemental File[1]) show variability in SiO_2, Al_2O_3, and CaO. Six samples (09TBT01, SUTHER, 12ZA61, 14ZA121, 14ZA128, 14ZA129) with high CaO (>5 wt%), low SiO_2 (<50 wt%), and high LOI (>10 wt%) are likely to contain minor secondary calcite and are excluded from further discussion because their compositions may have been affected by secondary diagenetic alteration. The remaining analyses (n = 35) were normalized to oxide totals (LOI excluded). Samples containing no significant calcite have SiO_2 between 47% and 73%, Al_2O_3 between 12% and 30%, CaO < 5%, NaO < 5%, K_2O from 1% to 7%, and P_2O_5 typically <1%. FeO values are reported as total Fe and range between 1% and 7%. MnO content is <0.3% and MgO varies slightly between 0.5% and 2.5%, with most values between 1% and 2%. TiO_2 is between 0.2% and 0.9% for all samples. Little variation is observed between the geochemistry of samples from the Beaufort and Ecca Groups in major element geochemistry.

South Africa Tuff XRF and ICPMS *(this study)*

	SiO2	TiO2	Al2O3	FeO*	MnO	MgO	CaO	Na2O	K2O	P2O5	LOI (%)	Sum
14ZA161A	68.38	0.595	15.72	3.67	0.046	1.02	0.24	0.66	3.39	0.025	5.71	99.46
14ZA162A	63.59	0.597	16.62	3.92	0.062	1.47	1.20	0.90	3.62	0.129	7.45	99.56
14ZA168A	62.67	0.735	17.14	5.22	0.049	1.40	0.47	1.40	4.55	0.086	5.45	99.16
13ZA93A-PWD	60.12	0.880	17.02	7.35	0.078	2.04	0.87	1.76	4.47	0.094	4.96	99.66
14ZA130A	62.72	0.789	17.14	4.78	0.046	1.68	0.65	0.98	4.44	0.229	6.03	99.47
14ZA130A R	62.47	0.788	17.01	4.75	0.046	1.67	0.71	0.98	4.42	0.229	6.03	99.10
14ZA130A	62.72	0.789	17.14	4.78	0.046	1.68	0.65	0.98	4.44	0.229	6.03	99.47
14ZA130A	62.20	0.801	17.34	5.11	0.056	1.71	0.66	0.92	4.51	0.239	6.07	99.62
~~SUTHER~~	~~38.06~~	~~0.329~~	~~16.38~~	~~3.45~~	~~0.603~~	~~1.67~~	~~14.90~~	~~1.11~~	~~3.67~~	~~0.128~~	~~18.54~~	~~98.83~~
~~13ZA72A~~	~~8.17~~	~~0.113~~	~~3.01~~	~~0.98~~	~~0.012~~	~~1.53~~	~~46.17~~	~~0.11~~	~~0.61~~	~~0.082~~	~~38.25~~	~~99.03~~
14ZA129A	50.32	0.573	14.08	3.77	0.106	1.70	11.44	0.58	3.40	0.127	13.56	99.65
BLOUKRANS	58.43	0.557	16.56	3.59	0.141	1.79	5.23	2.07	3.98	0.312	7.24	99.91
14ZA129A	56.50	0.661	16.54	4.47	0.096	2.00	5.12	0.54	4.11	0.133	9.33	99.49
12ZA45	63.41	0.524	17.13	3.39	0.024	1.64	0.82	1.22	3.50	0.107	7.46	99.22
14ZA128A	53.95	0.531	12.23	2.88	0.080	2.23	10.90	1.69	3.18	0.335	11.74	99.76
14ZA128A	54.43	0.547	12.53	3.08	0.079	2.32	9.76	1.68	3.23	0.334	11.14	99.13
12ZA46	63.21	0.625	16.67	5.59	0.046	1.66	1.41	0.94	4.48	0.157	5.19	99.98
13ZA75B-PWD	65.20	0.566	16.89	3.83	0.099	1.25	1.48	1.63	2.84	0.165	5.81	99.75
~~12ZA16-WT-L~~	~~42.69~~	~~0.402~~	~~11.76~~	~~2.26~~	~~0.055~~	~~1.67~~	~~17.82~~	~~1.16~~	~~2.92~~	~~0.741~~	~~17.66~~	~~99.14~~
13ZA76	60.96	0.666	17.76	4.10	0.038	1.99	1.23	1.81	4.63	0.109	6.56	99.86
~~12ZA12~~	~~23.45~~	~~0.289~~	~~5.98~~	~~1.90~~	~~0.281~~	~~0.96~~	~~35.14~~	~~0.71~~	~~1.43~~	~~0.124~~	~~29.02~~	~~99.28~~
13ZA77-PWD	69.29	0.641	13.57	3.05	0.230	1.08	2.58	2.37	2.31	0.213	4.92	100.25
12ZA07	56.05	0.686	20.89	4.71	0.081	1.90	1.29	1.21	4.88	0.187	7.90	99.79
12ZA23	50.90	0.210	26.33	2.78	0.024	2.21	0.43	0.21	7.95	0.037	7.91	98.98
14ZA116A	48.52	0.374	26.46	2.10	0.051	1.77	2.24	0.41	7.53	0.057	9.21	98.72
12ZA22A	53.42	0.615	21.71	6.24	0.059	2.48	0.97	1.56	5.35	0.135	7.35	99.89
12ZA22B	52.56	0.260	23.05	3.40	0.234	2.16	2.06	0.35	7.15	0.052	8.25	99.53
13ZA78A	50.43	0.451	13.72	2.25	0.238	1.04	13.68	2.57	2.77	0.135	12.79	100.08
~~12ZA08~~	~~22.15~~	~~0.361~~	~~11.80~~	~~1.19~~	~~0.531~~	~~1.04~~	~~30.89~~	~~0.06~~	~~3.58~~	~~0.023~~	~~27.68~~	~~99.30~~
~~14ZA121~~	~~44.70~~	~~0.323~~	~~23.04~~	~~2.73~~	~~0.244~~	~~1.80~~	~~7.10~~	~~0.33~~	~~6.82~~	~~0.091~~	~~11.43~~	~~98.60~~
~~14ZA141~~	~~14.43~~	~~0.164~~	~~5.65~~	~~1.68~~	~~0.546~~	~~1.40~~	~~39.81~~	~~0.35~~	~~1.16~~	~~0.164~~	~~33.90~~	~~99.25~~
12ZA54	47.55	0.697	26.44	4.37	0.109	2.04	2.09	0.39	6.74	0.305	8.89	99.61
12ZA61	52.75	0.696	18.62	8.52	0.307	1.39	1.50	1.05	2.64	0.225	11.55	99.25
09LGV-04	49.93	0.722	24.93	4.73	0.068	2.22	1.29	1.27	6.24	0.306	6.97	98.68
12ZA10	47.92	0.269	25.00	2.74	0.138	1.96	3.67	0.83	6.79	0.077	9.77	99.17
09LGV-01	58.26	0.414	22.36	1.97	0.016	1.56	1.44	0.66	6.20	0.190	6.26	99.32
13ZA79	73.17	0.483	14.57	1.67	0.011	0.67	0.68	3.77	2.10	0.124	3.10	100.34
~~09TBT-04~~	~~35.22~~	~~0.417~~	~~19.86~~	~~2.06~~	~~0.618~~	~~1.06~~	~~16.39~~	~~0.16~~	~~5.17~~	~~0.060~~	~~17.65~~	~~98.66~~
09LGV-02	51.69	0.656	25.59	3.60	0.022	1.93	0.70	1.24	6.82	0.157	7.02	99.44
14ZA154	58.89	0.683	18.58	6.26	0.026	1.56	0.39	0.38	3.93	0.162	9.06	99.91
14ZA154	61.12	0.620	17.02	6.35	0.030	1.46	0.39	0.56	3.82	0.156	7.49	99.03
~~09TBT-01~~	~~44.04~~	~~0.369~~	~~23.69~~	~~2.16~~	~~0.080~~	~~1.45~~	~~9.23~~	~~0.92~~	~~5.26~~	~~0.108~~	~~13.01~~	~~100.31~~
14ZA142	71.43	0.272	13.01	3.55	0.071	0.44	1.15	4.18	1.09	1.033	3.89	100.11
14ZA142 R	71.83	0.273	13.13	3.58	0.072	0.43	1.15	4.22	1.09	1.040	3.89	100.72
14ZA142	71.43	0.272	13.01	3.55	0.071	0.44	1.15	4.18	1.09	1.033	3.89	100.11
14ZA142	69.57	0.287	13.22	4.03	0.054	0.53	1.65	3.66	1.35	1.364	4.31	100.03
09LGC-04	50.52	0.490	24.56	3.23	0.125	1.64	2.60	1.69	6.32	0.291	7.22	98.67
09LGC-01	53.69	0.482	26.80	1.94	0.030	1.29	0.45	2.05	6.25	0.198	5.55	98.73
12ZA55	57.56	0.431	23.70	2.06	0.077	1.47	1.27	0.21	6.05	0.184	6.88	99.88
12ZA19	46.76	0.543	29.77	0.88	0.044	0.55	2.84	0.87	5.17	0.686	9.33	97.43

[1]Supplemental File. Four data tables that provide: (1) Whole-rock geochemistry from ICP-MS and XRF analysis; (2) U-Pb and REE from zircon SHRIMP analyses; (3) Ti in zircon temperatures; and (4) UTM Sample locations (WGS84). Please visit http://dx.doi.org/10.1130/GES01215.S1 or the full-text article on www.gsapubs.org to view the Supplemental File.

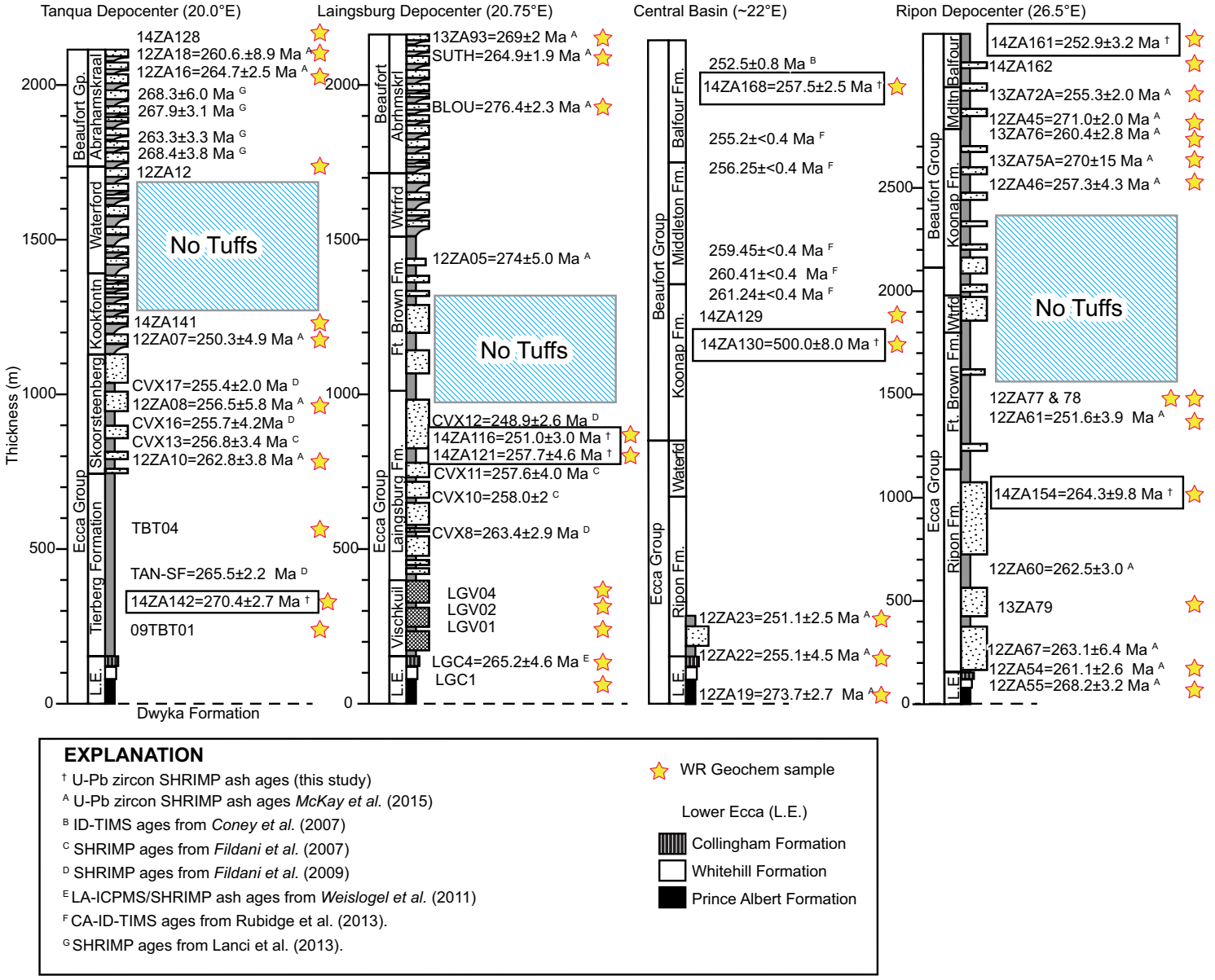

Figure 2. Chronostratigraphic constraints on the Karoo Supergroup strata based on U-Pb zircon geochronology of volcanic tuffs. Ecca Group tuffs young upward and tuffs in the uppermost Ecca Group are reproducibly younger than in the zircon-poor tuffs of the Beaufort Group (McKay et al., 2015). A tuff gap is regionally present, typically found directly above tuffs that yield a ca. 251 Ma age, which would correspond to the Permian-Triassic boundary. Tuff maximum depositional ages reported in this study have boxes around them and corroborate previously published age controls. SHRIMP—sensitive high-resolution ion microprobe; LA-ICP-MS—laser ablation–inductively coupled plasma–mass spectrometer; ID-TIMS—isotope dilution–thermal ionization mass spectrometry; CA—chemical abrasion; WR—whole rock; Gp—group; Fm—formation.

Trace element results, including REEs (Figs. 3A–3H) also show no distinguishing characteristics between the Ecca and Beaufort Group tuffs. Ecca Group tuffs show more compositional variability than the overlying Beaufort Group tuffs in Nb (ppm), Zr (ppm), Y (ppm), Rb (ppm), Yb (ppm), and Ce (ppm). Both the Ecca and Beaufort tuffs have negative sloped REE patterns with minor negative Eu anomalies. The most prominent Eu anomalies are two positive Eu anomalies, both found in Ecca tuffs. Five Beaufort tuffs also contain negative Ce anomalies and one Beaufort tuff contained a positive Ce anomaly; no Ce anomalies were observed in Ecca tuffs.

ZIRCON U-Pb AGES AND REE COMPOSITIONS

Methods

We sampled 29 tuffs from 4 transects through formations of the Ecca and Beaufort Groups exposed along the southern Karoo Basin (Fig. 1). Zircon grains were separated from samples using mineral separation techniques, including the use of a Franz magnetic separator to remove magnetically susceptible zircon that may have higher U and are likely to be metamict and/or yield discordant results (Sircombe and Stern, 2002). Zircon yields were variable for different samples, ranging between 0 and >200 zircons. Size, morphology, and inclusion density were not considered when selecting zircon for analysis in an effort to characterize the entire zircon population of a tuff and not bias results toward prismatic, acicular, euhedral zircon populations. Zircon grains were mounted in epoxy and polished to expose an interior cross section of the grain. Cathodoluminescence images were used to avoid inclusions and complex cores, and to target intermediate gray (corresponding to U concentration between 100 and 1000 ppm), oscillatory zoned rim domains for in situ zircon analyses. In situ zircon analyses were performed on the SHRIMP-RG (reverse geometry) ion microprobe at the Stanford University Microscopic Analytical Center under analytical conditions similar to those of Barth and Wooden (2010). The primary ion beam (O_2^-) was focused to a spot diameter between 18 and 22 µm in diameter, a depth of ~1.5 µm for analyses performed in this study. U-Pb ages were calculated with reference to the R33 and Temora zircon standards (419.3 and 416.8 Ma, respectively; Black et al., 2004). Zircon trace elements, including Y, La, Ce, Nd, Sm, Eu, Gd, Tb, Dy, Er, Yb, Lu, Hf, Th, and U were measured concurrently with U-Pb analyses and calibrated with the compositional zircon standard MADDER (Barth and Wooden, 2010). Model ages and trace element concentrations were calculated using the SQUID 2.51 (Ludwig, 2009) and ISOPLOT 3.76 software (Ludwig, 2012). The $^{206}Pb/^{238}U$ ages are corrected for common Pb (using ^{207}Pb assuming $^{206}Pb/^{238}U$-$^{207}Pb/^{235}U$ age concordance) and a model Pb composition from Stacey and Kramers (1975), with no additional error propagated from the uncertainty in the model common Pb composition (Pb_c). On average, zircon analyses contained >99.5% radiogenic Pb and the common Pb correction was negligible.

Of the 590 total individual grain analyses, 520 were accepted, ranging from 2607 to 226 Ma on the basis of low common Pb concentrations, low analytical uncertainty (<3%), and concordance. Grains were determined to be concordant if $^{238}U/^{206}Pb$ and $^{207}Pb/^{206}Pb$ ages overlapped within 2σ uncertainty. To determine maximum depositional ages, anomalously old zircon ages (older than 300 Ma) are interpreted as inherited xenocrystic or detrital contamination, while zircon with anomalously young ages (much older than ca. 250 Ma), high U (>1000 ppm), or high common Pb are dismissed as having been affected by Pb loss or common Pb contamination. Zircon age populations were identified using Kernel density estimate plots to interpret the youngest coherent population within a tuff. A weighted mean age was calculated from the youngest coherent population of concordant grains (>3 grains) to determine tuff maximum depositional ages. Uncertainties for weighted mean ages are presented as 2σ, including internal and external error. We report REE compositions for the 469 U-Pb zircon ages from 22 volcanic tuffs reported in McKay et al. (2015) and an additional 121 U-Pb zircon ages and REE compositions from 7 new tuff samples (Table 2 in the Supplemental File). There is no geographic relationship observed in U-Pb ages or REE zircon compositions. Zircon U-Pb ages, however, show stratigraphic trends, and therefore samples are presented based on stratigraphic position.

U-Pb Zircon Maximum Depositional Ages

The 121 newly obtained U-Pb zircon ages provide estimates for the maximum depositional age of 7 volcanic tuffs from the Karoo Basin: 1 sample from the southwestern Karoo near Robertson, Western Cape, 2 tuffs from the Laingsburg depocenter in the western Karoo Basin, 2 tuffs from the central Karoo Basin, and 2 tuffs from the Ripon depocenter in the eastern Karoo Basin (Universal Transverse Mercator locations in Table 3 in the Supplemental File).

Ecca Group

Four tuff samples were collected from within the Ecca Group. Sample 14ZA142 was collected from the lower Ecca Group within a structural inlier of Karoo Supergroup strata within the Cape fold belt near Robertson (Western Cape). The two youngest individual zircon ages are 226 ± 6 and 256 ± 9 Ma, but have relatively high analytical uncertainties (~3%, 1σ) and do not define a population. Therefore, the youngest, coherent population yields an age of 270.4 ± 2.7 Ma (2σ, n = 5, mean square of weighted deviates, MSWD = 2.1). Sample 14ZA121 was collected from a green, clay-rich tuff near Laingsburg (Western Cape) from the middle to upper Laingsburg Formation contained zircon that ranged in age between 1036 and 220 Ma. A subpopulation of 6 low common Pb, concordant grains yielded a weighted mean age of 257.7 ± 4.6 Ma, with an MSWD of 3.7. Zircon from 14ZA116, sampled from a clay-rich

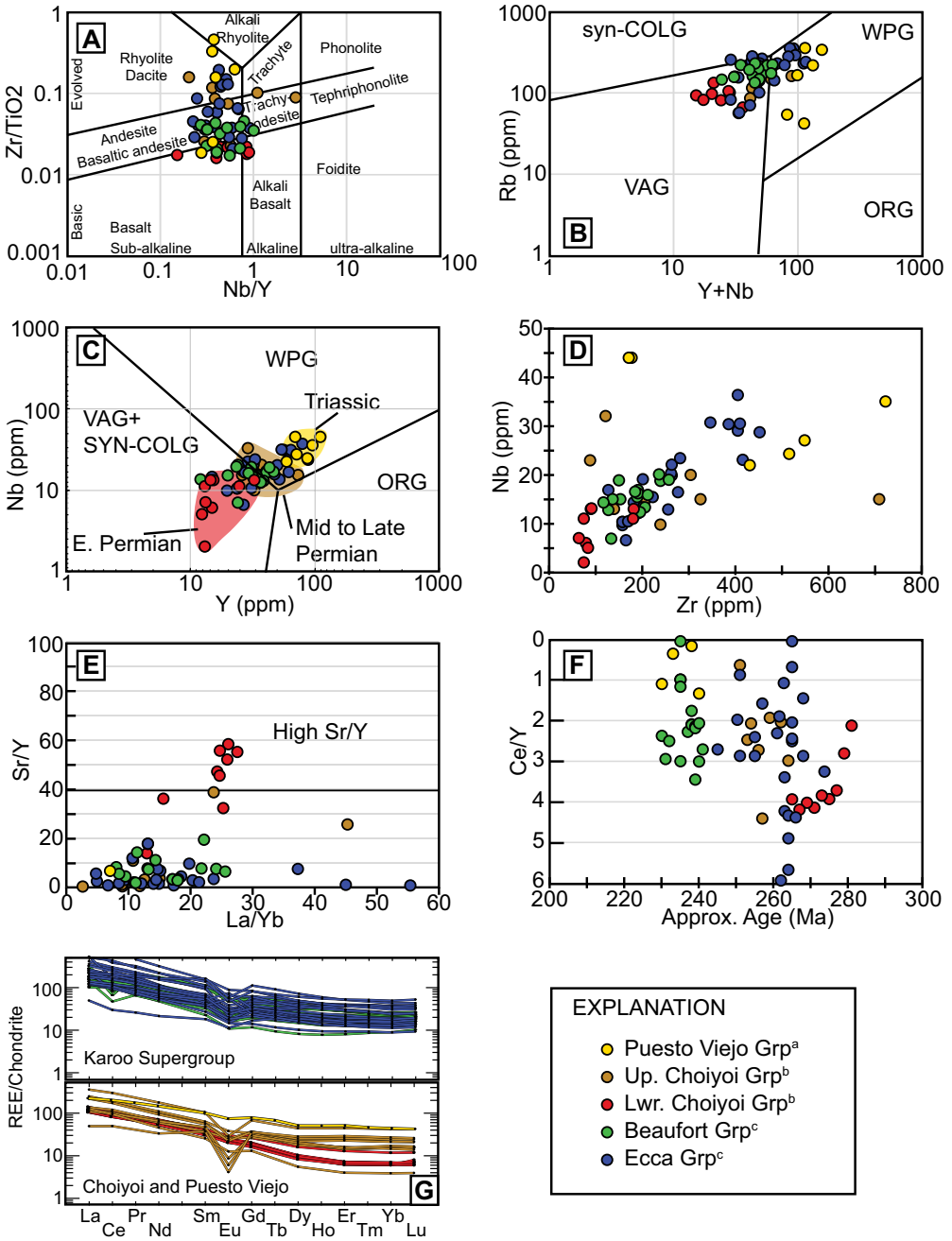

Figure 3. Whole-rock geochemistry of Karoo tuffs plotted with geochemistry from the Choiyoi Group (Kleiman and Salvarredi, 2001; Kleiman and Japas, 2009) and Puesto Viejo (Kleiman and Salvarredi, 2001) volcanic deposits in South America. Lwr.—lower; Grp—group. (A) Zr/TiO_2 versus Nb/Y with geochemical discrimination diagram of Winchester and Floyd (1977). (B) Rb versus Y + Nb. COLG—collision granites; WPG—within plate granites; VAG—volcanic arc granites; ORG—ocean ridge granites. (C) Nb versus Y with discrimination diagram of Pearce et al. (1984). E.—early. (D) Nb versus Zr. (E) Sr/Y versus La/Yb. (F) Ce/Y versus approximate age. (G) Chondrite normalized rare earth elements (REE).

tuff in the upper Laingsburg Formation, ranged in age from 1888 to 228 Ma. From 40 total analyses, 31 were Permian–Triassic in age. A population of 10, low common Pb, concordant grains yield a weighted mean age of 250.0 ± 2.1 Ma with an MSWD = 3.7. These two ages strongly suggest a late Permian to Early Triassic maximum depositional age for the upper Laingsburg. Sample 14ZA154 was collected from the middle Ripon Formation of the Ecca Group near Grahamstown (Eastern Cape) and contained zircons ranging in age from 1596 to 230 Ma. The weighted mean age of the youngest coherent zircon population is 264.3 ± 9.8 Ma (n = 5, MSWD = 3.5).

Beaufort Group

Three samples were collected from the Beaufort Group. Sample 14ZA130 was collected from a light brown tuff in the upper Abrahamskraal-Koonap Formation within the Beaufort Group ~25 km southeast of Fraserburg, along the Northern Cape–Western Cape border. This tuff yielded only 8 zircons, none of which were Permian–Triassic in age. The youngest grain within 14ZA130 was late Cambrian, 497 ± 6 Ma (1σ), an age not uncommon for Permian–Triassic tuffs in the Karoo Supergroup (McKay et al., 2015) or in age-correlative volcanics in South America (Domeier et al., 2011). Sample 14ZA168, collected ~16.1 km north of Graaff-Reinet (Eastern Cape), in the middle Balfour Formation yielded zircon that ranged in age between 1620 and 252 Ma. Permian grains dominate this sample (n = 19 of 30; 63%). A coherent population of 11 concordant, low common Pb grains produce a weighted mean age of 257.5 ± 2.5 Ma (MSWD = 1.43), which serves as the maximum deposition age for the Balfour Formation. Sample 14ZA161 was collected ~10 km northeast of Seymour (Eastern Cape) from the Balfour Formation of the Beaufort Group and contained zircon ranging in age from 2655 to 219 Ma. A small population of 5 low common Pb, concordant zircons produce a weighted mean age of 255.4 ± 3.1 Ma with an MSWD = 1.8.

Trace Elements in Zircon

To understand Permian–Triassic magmatism, we focus on the geochemical composition of 364 zircons that produced U-Pb ages younger than 300 Ma. Zircon data are subdivided into four age groups: early Permian (300–270 Ma), middle Permian (270–260 Ma), late Permian (260–251 Ma), and Triassic (younger than 251 Ma) (Fig. 4). Mean Hf_{zircon} concentration decreases from ~9300 ppm (1σ standard deviation, SD = 1794 ppm) in the early Permian, to 8991 and 8943 ppm (1σ SD = 1605, 1497 ppm) in the middle and late Permian, to 7679 ppm (1σ SD = 1585 ppm) in the Early Triassic (Fig. 4A), while median Hf_{zircon} values are within 150 ppm of mean values and display the same decreasing trend through time. Mean chondrite normalized Yb/La_{zircon} decreases (Fig. 4B) from 11,687 in the early Permian to 8092 in the middle Permian, and from 4507 in the late Permian to 2643 in the Early Triassic. Median Yb/La_{zircon} also systematically decreases with values of 4164, 3145, and 2011 in the early, middle, and late Permian, respectively, and 407 in the Triassic. Mean Ce/Ce^*_{zircon} also systematically decreases (Fig. 4C) from 51 (1σ SD = 70) in the early Permian, to 41 (1σ SD = 61) in the middle Permian, to 34 (1σ SD = 45) in the late Permian, to 9 (1σ SD = 11) in the Early Triassic, mirrored by median values that decrease from 24, 20, and 14 through the Permian to 6 in the Triassic. Mean Hf/Lu_{zircon} decreases through the Permian from 156 (1σ SD = 219) in the early Permian to 113 (1σ SD = 88) in the middle and late Permian and dropped to 70 (1σ SD = 67) in the Early Triassic, while median Hf/Lu_{zircon} values also decrease from 123 in the early Permian to ~100 in the middle and late Permian to 57 in the Early Triassic. Chondrite normalized Eu/Eu^*_{zircon} (Fig. 4E) does not vary significantly through time, with early, middle, and late Permian and Early Triassic grains producing mean values of ~0.38 (1σ SD = ~0.17); however, median values increase slightly from 0.37 in the early and middle Permian to ~0.40 in the late Permian and Triassic. Mean Th/U_{zircon} values increase slightly through time from 0.64 (1σ SD = 0.28) in the early Permian to 0.76 (1σ SD = 0.33) and 0.72 (1σ SD = 0.25) in the middle and late Permian and 0.77 (1σ SD = 0.31) in the Triassic. Median Th/U_{zircon} displays the same trend, although median values are 0.03–0.06 lower than mean values. The Ecca and Beaufort Group tuffs contain elevated Th/U (>1.0) zircons. Beaufort Group tuff zircons, however, contain a larger population of higher Th/U (>1.5) zircons, while few Ecca Group tuff zircons exceed Th/U ≥ 1.5.

Ti in Zircon

The incorporation of Ti into zircon has been shown to be controlled, in part, by the temperature during crystallization (Watson and Harrison, 2005; Watson et al., 2006; Hiess et al., 2008). Concentrations of Ti in zircon were collected for 77 zircons from 6 tuffs concurrent with U-Pb and REE analyses. Zircon analyses with elevated common Pb ($^{204}Pb/^{206}Pb > 0.0005$) and high Fe concentrations (>300 ppm) were excluded, leaving 51 Permian–Triassic Ti_{zircon} analyses. Ti_{zircon} model temperatures were calculated based on Si (a_{Si} = 1.0) and Ti (a_{Ti} = 0.7) activities from Claiborne et al. (2010). At an uncertainty of ± 0.2 in Si and Ti activities, temperature estimates could fluctuate ±30–40 °C; however, our interpretations are based on the relative temperature trends between samples, and therefore are less affected by this uncertainty. The Ti_{zircon} temperatures range from ~620 °C to >800 °C, with ±~10% uncertainty in each analysis. As a whole, the variability observed in Ti_{zircon} temperatures is minor throughout the Permian and Early Triassic, and all the Permian to Triassic average model temperatures are within uncertainty of one another. Ti_{zircon} indicates temperatures 796 ± 4 °C (n = 3) for 285–276 Ma zircon. Temperatures decreased into the middle Permian, where Ti_{zircon} temperatures average 747 ± 43 °C (1σ). Late Permian Ti_{zircon} temperatures are slightly higher with an average of 757 ± 37 °C (1σ). Early Triassic temperature estimates are slightly higher, with an average Ti_{zircon} temperature 760 ± 19 °C (1σ), although the latter is based on 5 grains.

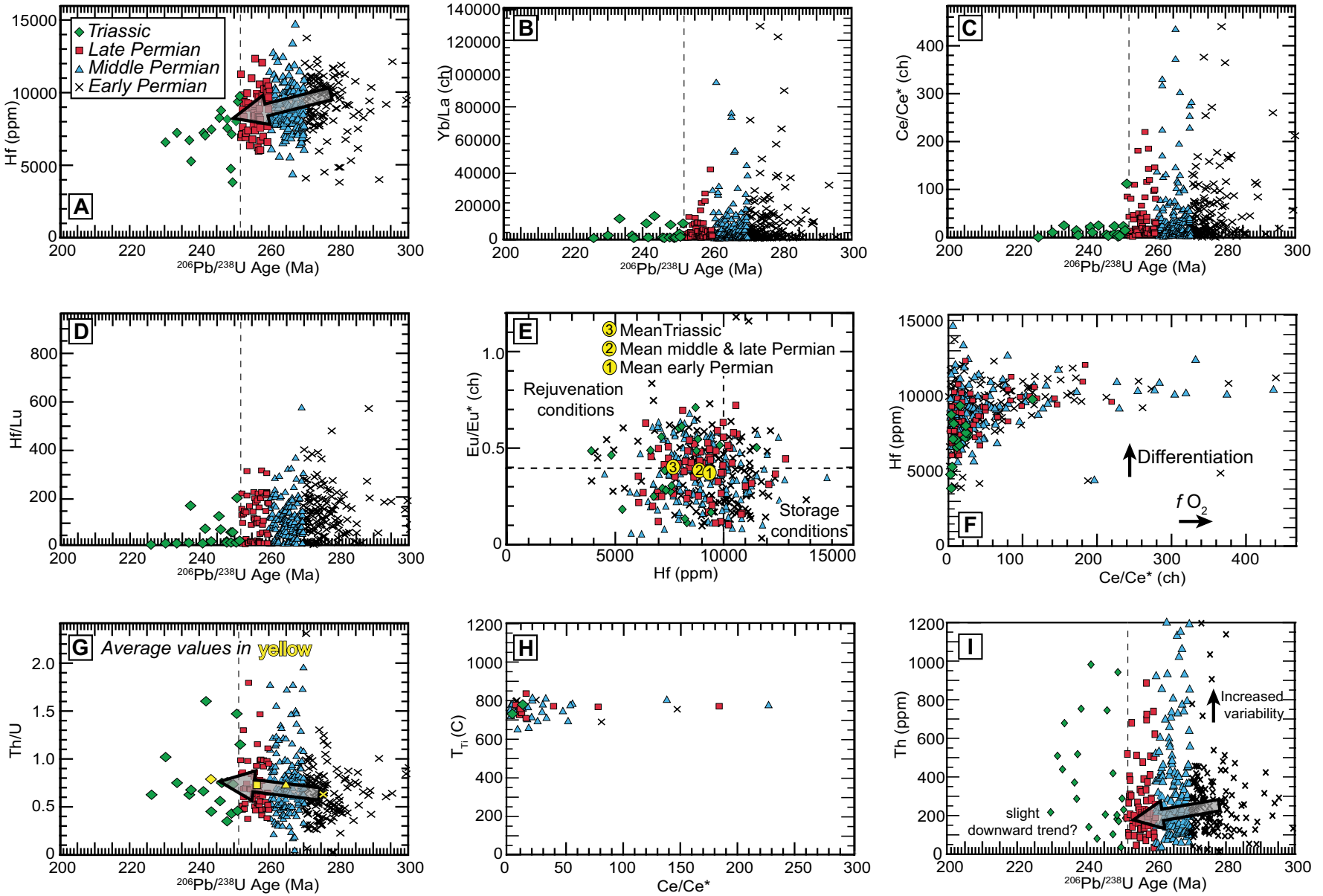

Figure 4. Zircon geochemistry and U-Pb ages show temporal trends in chemistry from Permian–Triassic zircons within Karoo Supergroup tuffs. (A) Hf (ppm). (B) Yb/La (ch—chondrite normalized). (C) Ce/Ce*. (D) Hf/Lu decrease through time. (E) Eu/Eu* vs. Hf (ppm) may contain a cryptic trend toward high Eu/Eu* and lower Hf (ppm) through time. (F) Hf and Ce/Ce* are, on average, lower and less variable in late Permian and Early Triassic zircon. (G) Th/U increases through time, with high Th/U (>1.0) zircon only occurring after the middle Permian (after 270 Ma). (H) Ti_{zircon} temperatures (*T*) are all within error and show no trends with Ce/Ce*. (I) Th (ppm) is increasingly variable after ca. 275 Ma with some elevated Th zircon; however, the bulk trend slightly decreases through time.

DISCUSSION

Zircon geochemistry can record the prolonged petrogenetic history of a magmatic system (Claiborne et al., 2010; Schoene et al., 2012) that may differ from the whole-rock chemistry of volcanic tuffs. Whole-rock chemistry is susceptible to posteruptive alteration by hydrothermal and weathering processes (Hastie et al., 2007), whereas zircon may preserve a more robust record of magmatic composition. Therefore, whole-rock and zircon geochemistry are discussed separately.

Petrogenesis of Karoo Tuffs from Whole-Rock Geochemistry

A traditional technique to geochemically differentiate the tectonic source of igneous rocks is by using discrimination diagrams, where igneous suites from well-characterized tectonic settings are used to defined geochemical fields. These fields commonly overlap and the results can be ambiguous or misleading in complex magmatic systems (Förster et al., 1997). Because this approach has been used to classify volcanic igneous suites in age-equivalent rocks from elsewhere in Gondwana (Kleiman and Japas, 2009), we use granitoid discrimination diagrams from Pearce et al. (1984) to attempt to distinguish the source for distal ashes exposed in the Karoo Basin based on tuff whole-rock geochemical composition. Tuffs from the Ecca and Beaufort Groups in the Karoo Supergroup are nearly indistinguishable based on whole-rock geochemical signatures. Because major element composition may be easily altered (Hastie et al., 2007), immobile trace elements may better preserve the original composition of the tuff (Floyd and Winchester, 1978). Variability in Zr/TiO_2 between ~0.01 and 0.2 (Fig. 3A; Winchester and Floyd, 1977) suggests that the Ecca tuffs ranged between dacitic and basaltic compositions, while Beaufort tuffs are basaltic to andesitic in composition. Low Nb/Y (<1) may reflect subalkaline compositions for both the Ecca and Beaufort tuffs. Beaufort Group tuffs show less geochemical variability in Nb, Zr, Y, and Rb, but the Ecca and Beaufort Group tuffs plot between the volcanic arc and intraplate (within plate granites) granitoid fields of Pearce et al. (1984) (Figs. 3B, 3C). This is distinct from the arc-driven magmatism of the lower Choiyoi Group rocks in South America (Kleiman and Japas, 2009) which have lower Nb, Zr, Rb, and Y concentrations that plot (Figs. 3B, 3C) in the volcanic arc and syncollisional granitoid fields of Pearce et al. (1984). Karoo tuffs generally have low Sr/Y (<20), La/Yb (<25), and Ce/Y (<4) values. Based on similar Nb (>10 ppm), Zr (>100 ppm), Rb (>100 ppm), Y (>60), Sr/Y (<25), La/Yb (<25), and Ce/Y (<4) values, Karoo Supergroup tuffs are most similar to upper Choiyoi volcanism, which has been interpreted to be the product of postorogenic collapse (Kleiman and Japas, 2009). Karoo Supergroup tuffs, like upper Choiyoi and Puesto Viejo volcanics, contain low Sr/Y (<40) (Fig. 3E), which is likely sourced from primitive melts that form in the absence of garnet, suggesting shallow, low-pressure magmatic sources (Moyen, 2009). Several early Permian (before 260 Ma) tuffs from the Karoo Supergroup have elevated Ce/Y (>3.5), which is similar to early Permian lower Choiyoi Group volcanism (Ce/Y 2–4.5). Ce/Y serves as proxy for the ratio of light (L) to heavy (H) REEs (Mantle and Collins, 2008). The majority of Karoo tuffs, like the upper Choiyoi and Puesto Viejo volcanics have lower Ce/Y (<3.5) (Fig. 3F). The transition from high Sr/Y (>40), high Ce/Y (>3.5) in the early Permian to lower Sr/Y (<20), lower Ce/Y (<3.5) could suggest that primitive melt sources that fed Permian–Triassic volcanism in western Gondwana came from increasingly shallower crustal depths for the Karoo, upper Choiyoi, and Puesto Viejo volcanic suites. The observed transition from high Sr/Y, high Ce/Y melts in the early Permian to lower Sr/Y, Ce/Y melts in the middle Permian through Early Triassic in South American igneous suites coincides with an interpreted shift from arc to extensional magmatism (Kleiman and Japas, 2009). Although no high Sr/Y tuffs were identified in the Karoo Supergroup, Karoo tuffs show a similar transition from high Ce/Y melts in the early Permian (Ecca Group) to low Ce/Y in the late Permian (Ecca) and Early Triassic (Beaufort) Karoo Supergroup. Negative Eu anomalies in upper Choiyoi Group rocks and negative and positive Eu anomalies in Karoo tuffs (Fig. 3G) suggest the presence of plagioclase in a crustal melt source (Gao and Wedepohl, 1995) and/or fractionation of plagioclase (Rudnick, 1992) during the evolution of Permian melts. This geochemical shift might represent an increasingly shallower melt source for the Karoo tuffs, similar to the transition from deep-sourced, arc-driven melting toward extensional magmatism that has been interpreted for South American volcanics. Although the similarity between South American and Karoo Supergroup tuffs suggests a common origin, a major shift toward extensional magmatism in southern Gondwana may have occurred along the entire margin. Geochemistry from Permian–Triassic basalts in southeastern Gondwana has suggested coeval, Permian–Triassic crustal thinning associated with a shift toward extensional magmatism (Mantle and Collins, 2008). Therefore, a transition from subduction-driven arc magmatism toward extensional magmatism is not distinctive in identifying volcanic source provenance in Permian–Triassic volcanic suites throughout southern Gondwana.

Zircon Petrochronology of Karoo Tuffs

Although whole-rock geochemistry of volcanic tuffs can provide insight into the petrogenetic history of a magmatic system, tuffs can be subject to postdepositional weathering, reworking and/or detrital mixing, and alteration that can change the whole-rock geochemistry (Gatti et al., 2014). Zircon trace element chemistry has been widely applied to characterize magma chamber processes because zircon chemistry reflects the equilibrium melt composition from which it crystallized (e.g., Barth and Wooden, 2010; Claiborne et al., 2010). Zircon geochemistry from the Permian–Triassic tuffs in the Karoo Supergroup provides an opportunity to explore the history of magmatism in southern Gondwana, independent from whole-rock geochemistry. Because zircon is much more resistant to weathering and alteration, the zircon composition may provide the most accurate information about the magmatic source composition of these tuff deposits.

The decreasing Hf concentration in zircon (Hf_{zircon}) from an average of ~9300 ppm in the early Permian to ~7700 ppm in the Triassic suggests that melts became primitive and less fractionated through time (Fig. 4A). The variability in Hf_{zircon} also decreases through time, suggesting less variable magmatic conditions. The decrease in mean Hf_{zircon} and Hf_{zircon} variability coincides with a minor increase in Eu/Eu*, which might correlate to a shift from cooler crystal-rich magmatism toward warmer magmatism that was more likely to recycle older crystal phases (Klemetti and Clynne, 2014), although there is significant overlap that makes this interpretation tenuous. The decrease in Ce/Ce*, from an average of 67 in the early Permian to an average of 12 in the Triassic (Fig. 4C), with no clear major change in Ti in zircon temperatures (Fig. 4H) suggests a decrease in fO_2 to more reducing magma conditions. This may represent a transition from arc magmatism toward backarc (e.g., intraplate) magmatism, since intraplate melts are more reduced than arc magmas (Kelley and Cottrell, 2009). Hf concentration and Ce/Ce*, proxies for melt evolution and fO_2, respectively, are highly variable throughout Permian and Triassic zircon; however, variability and mean/median values for Hf and Ce/Ce* decrease through time (Fig. 4F) with the lowest values present in the youngest Triassic zircon, suggesting less variable conditions in these more primitive, less hydrous melts. Average Th/U in zircon increases from ~0.65 in the early Permian to 0.77 by the Early Triassic, which is largely a result of an increasing number of high Th/U (>1.0) analyses, which are only present in grains younger than ca. 275 Ma. This suggests that middle to late Permian melts became less evolved, possibly due to derivation from a more mafic source. The increase in Th/U correlates with an apparent increase in the variability of Th (ppm) in zircon after 275 Ma (Fig. 4I). While elevated Th could correlate to either an increase in crustal contribution or fractionation of a mafic melt (Klemetti et al., 2014), bulk Th values do not change significantly (mean 272–379 ppm, median 215–288 ppm) through time and the minor overall decreasing trend of the tightly grouped, less variability, lower Th population (<500 ppm) is difficult to interpret.

More primitive, less evolved melts tend to have lower Si activity (i.e., quartz not present as a phenocryst) and generally have lower Zr concentration, as Zr is an incompatible trace element that generally increases with increasing melt evolution or differentiation. A shift toward more primitive melts (i.e., lower whole-rock Zr, increase in Th/U_{zircon}, and decreasing Hf and Ce/Ce* in zircon) may explain the lack of coeval zircon in Beaufort tuffs compared to the underlying Ecca tuffs. Ecca tuffs display a wide range of whole-rock Zr concentrations (132–453 ppm, mean 292 ppm) that are on average higher than in the overlying Beaufort tuffs (118–258 ppm; mean 187 ppm). Lower Zr compositions would lead to melts that are less likely to achieve Zr saturation, resulting in decreasing zircon crystallization. Ti_{zircon} model temperatures suggest that zircon from Karoo tuffs grew in melts between ~700 and 800 °C, and whole-rock Zr/TiO_2 versus Nb/Y compositions suggest that Karoo tuffs are subalkaline basaltic andesite in composition. The Zr saturation models of Watson and Harrison (1983) estimate that for a basaltic andesite (M [cation ratio] = ~1.7) at ~750 °C the minimum concentration of Zr required to crystallize zircon is ~135 ppm. That minimum concentration increases to ~240 ppm at 800 °C and 415 ppm at 850 °C (the upper range of Ti-in-zircon temperatures). Ecca Group tuffs are bimodal in composition with respect to Zr, with a low Zr population ranging from 129 to 283 ppm (mean 212 ppm) and a higher Zr population with concentrations between Zr 347–453 ppm (mean 403 ppm). The bimodal nature of Zr concentrations in Ecca tuffs suggests that during Permian volcanism, low Zr magmas may have been less likely to grow zircon, while periodic Zr saturation might have been achieved during influx of high Zr melts, resulting in zircon crystallization events. In contrast, Beaufort tuffs are consistently lower in Zr (118–257 ppm) and near or below Zr saturation concentrations with no evidence for episodic Zr replenishment; this suggests that little to no new zircon would crystallize in the magmatic source of the tuffs deposited in the Beaufort Group, particularly within melts above >750 °C. New zircon growth may have been restricted (or absent) during Beaufort-age magmatism, which would promote the occurrence of inherited grains in volcanic tuffs, as has been observed in Beaufort tuffs (McKay et al., 2015). Increased inheritance of zircon would also account for the difficulty in obtaining reliable U-Pb zircon depositional age constraints in Beaufort tuffs.

Zircon Correlation between South Africa and Gondwanan Suite

Zircon REE data are not available in the literature for correlative magmatic and volcanic suites from South American and Antarctica, and therefore correlations based on zircon chemistry are restricted to Th and U, since these elements are collected for all U-Pb zircon analyses. Th/U in zircon data measured by SHRIMP from South America (Spalletti et al., 2008; Rocha-Campos et al., 2011; Domeier et al., 2011; Barredo et al., 2012; Ottone et al., 2014) and Antarctica (Riley et al., 2012; Elliot et al., 2014, 2015) contain a variable range of Th/U in zircon, including a large number (n = 41 of 428 Permian–Triassic analyses) with high Th/U (>1). High Th/U (>1) in zircon may form in less evolved melts (Kirkland et al., 2015), while the presence of a wide range of Th/U compositions likely represents variable magmatic source chemistry (Barth et al., 2013) and/or crystallization temperatures (Kirkland et al., 2015). Mid-crustal plutons in the Antarctic peninsula (Riley et al., 2012) and volcaniclastic strata in the central Transantarctic and Ellsworth Mountains (Elliot et al., 2014, 2015) contain zircon with Th/U ranging from <0.01 to 1.7. High Th/U_{zircon} (>1.0) ranges from the early Permian (ca. 280 Ma) into the Early Triassic (Fig. 5). Zircons from Karoo tuffs also contain high Th/U_{zircon} (>1.0) that range from 280 to 240 Ma (n = 45 of 364; ~12%). This contrasts with Th/U_{zircon} from South American volcanic rocks, where high Th/U (>1.0) zircons are mostly restricted to Triassic, younger than 245 Ma grains (n = 17 of 186) associated with Puesto Viejo and Rincón rift magmatism. Puesto Viejo volcanism also recycled Choiyoi age zircon cargo (Fig. 5A) resulting in a bimodal population of low Th/U_{zircon} between 0.3 and 0.5 and high Th/U_{zircon} between 0.8 and 2.5. Similar high (>1.0) Th/U_{zircon} are observed in Beaufort Group and Ecca Group tuffs (Fig. 5B), but are 265–250 Ma, which is not compatible with it being sourced from South America, where 265–250 Ma zircons are almost entirely devoid of high Th/U (>1.0). We therefore propose

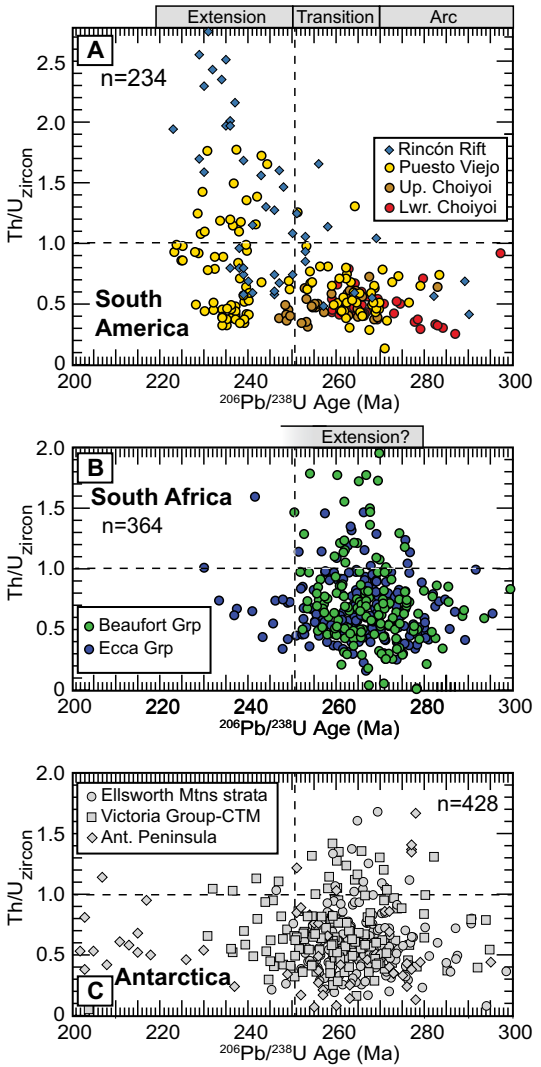

Figure 5. Th/U vs. U-Pb ages for Permian–Triassic zircon from South America (Spalletti et al., 2008; Rocha-Campos et al., 2011; Domeier et al., 2011; Barredo et al., 2012; Ottone et al., 2014), Karoo Supergroup, South Africa (this study), and Antarctica (Riley et al., 2012; Elliot et al., 2014, 2015). (A) High Th/U zircons (>1.0) in South America are related to Puesto Viejo and Rincón rift volcanism younger than 245 Ma. Up.—upper; Lwr.—lower. (B) Karoo tuffs also contain high Th/U zircons, but significantly older (275–255 Ma) than those in South America (Grp.—group). (C) Antarctic volcanogenic sediments also contain high Th/U Permian zircon, suggesting a correlation between Karoo tuffs and volcanism adjacent to Antarctica (Ant.). Higher Th/U (>1.0) zircons, which are present in extensional magmatism in South America, might reflect an early phase of extensional magmatism near Antarctica. CTM—central Transantarctic Mountains. Mtns—Mountains.

that high Th/U (>1.0) zircon might represent 265–250 Ma extensional magmatism elsewhere in Gondwana. Permian high Th/U zircons present in volcaniclastic suites from Antarctica (Fig. 5C) are geochemically and temporally compatible with sharing a magmatic source. While the whole-rock geochemistries of South American and Karoo Supergroup volcanic suites are comparable, the age-dependent Th/U zircon compositions are not. Based on zircon Th/U and U-Pb age, mid-crustal and volcanogenic sediment and/or tuffs from Antarctica most closely fit the age and composition of zircon in the Karoo Basin, suggesting that volcanic tuffs were sourced from Antarctica or elsewhere in Gondwana.

Implications for Gondwanan Tectonism

The whole-rock geochemistry of volcanic tuffs from the Karoo Supergroup suggests that the magmatic source for Karoo ashes was not a subduction-fed volcanic arc sourced from beneath the middle to lower crust (>40 km). In contrast, geochemistry suggests that the tuffs were sourced from a system transitioning toward intraplate volcanism, characterized by high Nb, Zr, Y, and lower Sr/Y, La/Yb, and Ce/Y. Intraplate, postorogenic to rift-related magmatism probably began by ca. 270 Ma within southern Gondwana, earlier than previously thought. Tuff geochemistry records low Sr/Y (<20) and Ce/Y (decreasing from as much as 5 in the middle Permian to <3 in the late Permian to Early Triassic), suggests a lack of garnet and melts less enriched in LREEs, respectively. We suggest that these observations reflect a shallowing of magmatism (Figs. 4G, 4H) that is geochemically compatible with backarc extensional volcanism (Fig. 4E). Zircon geochemistry further corroborates this hypothesis, with decreasing Hf (ppm) (Fig. 4A) suggesting more primitive, lower fO_2, less hydrous melts (Fig. 4C), which would be expected during a transition from convergent arc to extensional magmatism. High Th/U in Permian zircon may have a genetic history similar to that of Triassic rift-related zircon in the Puesto Viejo volcanics of South America, but predates Puesto Viejo magmatism. Therefore, a poorly understood backarc magmatic zone may be in the faulted half-graben blocks underneath the South American, Antarctic, or African continental shelves. Recent research in the Antarctic has inferred backarc extension between the Antarctic Peninsula and other outboard fragmented terranes of southern Gondwana and East Antarctica (Fig. 6; Elliot et al., 2014). Elliot et al. (2014) suggested the presence of Permian–Triassic backarc basins along the boundaries between (1) the Antarctic peninsula and South Africa–eastern Antarctica and (2) Marie Byrd Land and eastern Antarctica. The geochemical and geochronological data presented here support the presence of this hypothetical backarc magmatism in western Gondwana, although little direct physical evidence remains. Extensional magmatism in the Permian Antarctic-Karoo backarc appears to predate Triassic extensional magmatism in South America; Permian–Triassic rifting may have migrated westward over time. The development of a Permian–Triassic crustal weakness in the now-dissected crust of Gondwana may have ultimately played a role in the Jurassic rifting and break-up of the

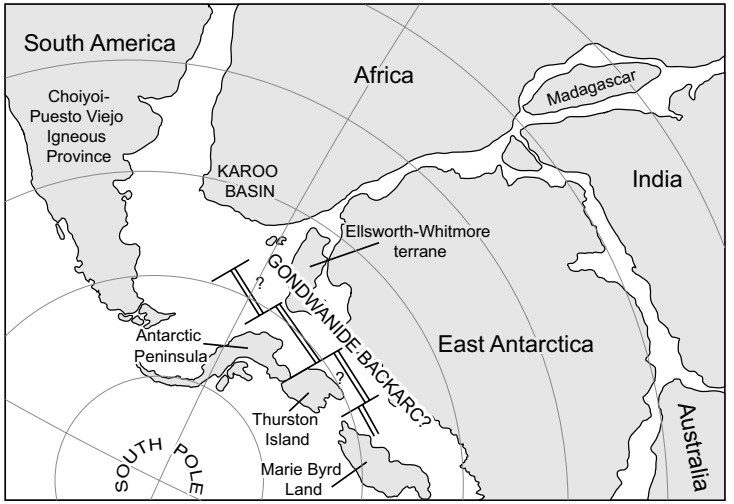

Figure 6. Paleogeographic schematic map of southern Gondwana with the location of possible backarc magmatism (Elliot et al., 2014) inboard of the Gondwanide magmatic arc.

supercontinent along those preexisting crustal boundaries. The break-up of Gondwana is typically considered to have begun along the boundary between Africa and Antarctica, just to the east of the Karoo Basin. The Karoo igneous province, located in the central Karoo Basin (Fig. 1), may be related to initial rifting of Gondwana (Encarnación et al., 1996; Jourdan et al., 2005). Jurassic rifting of western Gondwana would parallel the trend of the Permian–Triassic extensional feature, with the southern Atlantic and Southern oceans opening along the same crustal boundary in a similar southeast to northwest trend. The preexisting Permian–Triassic backarc is located at the triple junction along which South America, Africa, and Antarctica rift apart; this suggests that this missing tectonic feature may have played a pivotal role in the shaping the tectonic plate morphology and Mesozoic rifting of Gondwana.

CONCLUSIONS

Based on tuff whole-rock and zircon geochemistry and U-Pb geochronology, we propose that volcanic tuffs in the Karoo Basin may have been sourced by a postorogenic to rift extensional magmatic system. Although Karoo tuffs have been linked to age-correlative South American volcanism, zircon REE and Th/U geochemistry suggests that Karoo tuffs are genetically more similar to volcanic tuffs and volcanogenic sediment in Antarctica. Zircon geochemistry suggests that volcanism was sourced from increasingly reduced, primitive magmas in the middle to late Permian, while whole-rock geochemistry suggests shallower sourced melts in an intraplate setting. We interpret these observations to be consistent with backarc magmatism. With the intense tectonic dissection of southern Gondwana during Mesozoic opening of the Indian and Atlantic Oceans, large portions of the Gondwanan rock record are not accessible for field study and detailed geochemical-geochronology analyses, and no evidence for this possible backarc remains. Integrating U-Pb zircon and zircon REE geochemistry with whole-rock tuff geochemistry allows us to reconstruct the magmatic history of Gondwana and missing tectonographic provinces. This study demonstrates the utility of zircon U-Pb and REE analyses for U-Pb zircon provenance of volcanic tuffs to provide insight beyond whole-rock chemistry, which may be altered by posteruptive processes. Currently, the global lack of zircon geochemistry data sets hinders widespread use of integrated zircon U-Pb and geochemistry as a correlation tool. Advances in microanalysis in the near future may facilitate a proliferation of zircon geochemistry, greatly enhancing provenance techniques in sedimentology, petrology, and tephrochronology.

ACKNOWLEDGMENTS

This project was made possible through funding from West Virginia University, the American Association of Petroleum Geologists, the Society for Sedimentary Geology, the Geological Society of America, R. Shumaker, and the SLOPE4 Research Consortium managed by the University of Manchester and the University of Leeds. Reviews from Erik Klemetti, an anonymous reviewer, and guest editor Joshua Schwartz greatly improved this manuscript.

REFERENCES CITED

Bangert, B., Stollhofen, H., Lorenz, V., and Armstrong, R., 1999, The geochronology and significance of ash-fall tuffs in the glaciogenic Carboniferous–Permian Dwyka Group of Namibia and South Africa: Journal of African Earth Sciences, v. 29, p. 33–49, doi:10.1016/S0899-5362(99)00078-0.

Barboni, M., Schoene, B., Ovtcharova, M., Bussy, F., Schaltegger, U., and Gerdes, A., 2013, Timing of incremental pluton construction and magmatic activity in a back-arc setting revealed by ID-TIMS U/Pb and Hf isotopes on complex zircon grains: Chemical Geology, v. 342, p. 76–93, doi:10.1016/j.chemgeo.2012.12.011.

Barredo, S., Chemale, F., Marsicano, C., Ávila, J.N., Ottone, E.G., and Ramos, V.A., 2012, Tectono-sequence stratigraphy and U-Pb zircon ages of the Rincón Blanco depocenter, northern Cuyo Rift, Argentina: Gondwana Research, v. 21, p. 624–636, doi:10.1016/j.gr.2011.05.016.

Barth, A.P., and Wooden, J.L., 2010, Coupled elemental and isotopic analyses of polygenetic zircons from granitic rocks by ion microprobe, with implications for melt evolution and the sources of granitic magmas: Chemical Geology, v. 277, p. 149–159, doi:10.1016/j.chemgeo.2010.07.017.

Barth, A.P., Wooden, J.L., Jacobson, C.E., and Economos, R.C., 2013, Detrital zircon as a proxy for tracking the magmatic arc system: The California arc example: Geology, v. 41, p. 223–226, doi:10.1130/G33619.1.

Black, L.P., et al., 2004, Improved $^{206}Pb/^{238}U$ microprobe geochronology by the monitoring of a trace-element–related matrix effect; SHRIMP, ID–TIMS, ELA–ICP–MS and oxygen isotope documentation for a series of zircon standards: Chemical Geology, v. 205, p. 115–140, doi:10.1016/j.chemgeo.2004.01.003.

Chelle-Michou, C., Chiaradia, M., Ovtcharova, M., Ulianov, A., and Wotzlaw, J., 2014, Zircon petrochronology reveals the temporal link between porphyry systems and the magmatic evolution of their hidden plutonic roots (the Eocene Coroccohuayco deposit, Peru): Lithos, v. 198–199, p. 129–140, doi:10.1016/j.lithos.2014.03.017.

Claiborne, L.L., Miller, C.F., Flanagan, D.M., Clynne, M.A., and Wooden, J.L., 2010, Zircon reveals protracted magma storage and recycling beneath Mount St. Helens: Geology, v. 38, p. 1011–1014, doi:10.1130/G31285.1.

Cole, D.I., 1992, Evolution and development of the Karoo basin, *in* de Wit, M.J., and Ransome, I.G.D., eds., Inversion tectonics of the Cape fold belt, Karoo and Cretaceous basins of southern Africa: Rotterdam, Balkema, p. 87–100.

Coney, L., et al., 2007, Geochemical and mineralogical investigation of the Permian-Triassic boundary in the continental realm of the southern Karoo Basin, South Africa: Palaeoworld, no. 16, p. 67-104, doi:10.1016/j.palwor.2007.05.003.

Dahlgren, R., Shoji, S., and Nanzyo, M., 1993, Mineralogical characteristics of volcanic ash soils, *in* Shoji, S., eds., Volcanic ash soils: Genesis, properties, and utilization: Developments in Soil Science 21: Amsterdam, Elsevier, p. 101–144.

Dahlgren, R., Dragoo, J., and Ugolini, F., 1997, Weathering of Mt. St. Helens Tephra under a cryic-udic climate regime: Soil Science Society of America Journal, v. 61, p. 1519–1525, doi:10.2136/sssaj1997.03615995006100050032x.

DeCelles, P.G., 2011, Foreland basin systems revisited: Variations in response to tectonic settings, *in* Busby, C., and Pérez, A.A., eds., Tectonics of sedimentary basins: Recent advances: New York, Wiley-Blackwell Publishing, p. 405–426, doi:10.1002/9781444347166.ch20.

Domeier, M., Van der Voo, R., Tomezzoli, R.N., Tohver, E., Hendriks, B.W.H., Torsvik, T.H., Vizan, H., and Dominguez, A., 2011, Support for an "A-type" Pangea reconstruction from high-fidelity Late Permian and Early to Middle Triassic paleomagnetic data from Argentina: Journal of Geophysical Research, v. 116, B12114, doi:10.1029/2011JB008495.

Elliot, D.H., Fanning, C.M., and Laudon, T.S., 2014, The Gondwana plate margin in the Weddell Sea sector: Zircon geochronology of upper Paleozoic (mainly Permian) strata from the Ellsworth Mountains and eastern Ellsworth Land, Antarctica: Gondwana Research, doi:10.1016/j.gr.2014.12.001.

Elliot, D.H., Fanning, C.M., and Hulett, S.R.W., 2015, Age provinces in the Antarctic craton: Evidence from detrital zircons in Permian strata from the Beardmore Glacier region, Antarctica: Gondwana Research, v. 28, p. 152–164, doi:10.1016/j.gr.2014.03.013.

Encarnación, J., Fleming, T.H., Elliot, D.H., and Eales, H.V., 1996, Synchronous emplacement of Ferrar and Karoo dolerites and the early breakup of Gondwana: Geology, v. 24, p. 535–538, doi:10.1130/0091-7613(1996)024<0535:SEOFAK>2.3.CO;2.

Fildani, A., Drinkwater, N.J., Weislogel, A., McHargue, T., Hodgson, D.M., and Flint, S.S., 2007, Age controls on the Tanqua and Laingsburg deep-water systems: New insights on the evolution and sedimentary fill of the Karoo Basin, South Africa: Journal of Sedimentary Research, v. 77, p. 901–908, doi:10.2110/jsr.2007.088.

Fildani, A., Weislogel, A., Drinkwater, N.J., McHargue, T., Tankard, A., Wooden, J., Hodgson, D., and Flint, S., 2009, U-Pb zircon ages from the southwestern Karoo Basin, South Africa—Implications for the Permian-Triassic boundary: Geology, v. 37, p. 719–722, doi:10.1130/G25685A.1.

Floyd, P.A., and Winchester, J.A., 1978, Identification and discrimination of altered and metamorphosed volcanic rocks using immobile elements: Chemical Geology, v. 21, p. 291–306.

Förster, H.J., Tischendorf, G., Trumbull, R.B., 1997, An evaluation of the Rb vs. (Y + Nb) discrimination diagram to infer tectonic setting of silicic igneous rocks: Lithos, v. 40, p. 261–293, doi:10.1016/S0024-4937(97)00032-7.

Fruchter, J.S., et al., 1980, Mount St. Helens ash from the 18 May 1980 eruption: Chemical, physical, mineralogical, and biological properties: Science, v. 209, p. 1116–1125, doi:10.1126/science.209.4461.1116.

Gao, S., and Wedepohl, K.H., 1995, The negative Eu anomaly in Archean sedimentary rocks: Implications for decomposition, age and importance of their granitic sources: Earth and Planetary Science Letters, v. 133, p. 81–94, doi:10.1016/0012-821X(95)00077-P.

Gatti, E., Villa, I.M., Achyuthan, H., Gibbard, P.L., and Oppenheimer, C., 2014, Geochemical variability in distal and proximal glass from the Youngest Toba Tuff eruption: Bulletin of Volcanology, v. 76, p. 859–875, doi:10.1007/s00445-014-0859-x.

Gordon, S.M., Whitney, D.L., Teyssier, C., and Fossen, H., 2013, U-Pb dates and trace-element geochemistry of zircon from migmatite, Western Gneiss Region, Norway: Significance for history of partial melting in continental subduction: Lithos, v. 170–171, p. 35–53, doi:10.1016/j.lithos.2013.02.003.

Grimes, C.B., John, B.E., Kelemen, P.B., Mazdab, F.K., Wooden, J.L., Cheadle, M.J., Hanghoj, K., and Schwartz, J.J., 2007, Trace element chemistry of zircons from oceanic crust: A method for distinguishing detrital zircon provenance: Geology, v. 35, p. 643–646, doi:10.1130/G23603A.1.

Harvey, J.C., 2014, Zircon age and oxygen isotopic correlations between Bouse Formation tephra and the Lawlor Tuff: Geosphere, v. 10, p. 221–232, doi:10.1130/GES00904.1.

Hastie, A.R., Kerr, A.C., Pearce, J.A., and Mitchell, S.F., 2007, Classification of altered volcanic island arc rocks using immobile trace elements: Development of the Th/Co discrimination diagram: Journal of Petrology, v. 48, p. 2341–2357, doi:10.1093/petrology/egm062.

Heintz, M.L., Yancey, T.E., Miller, B.V., and Heizler, M.T., 2015, Tephrochronology and geochemistry of Eocene and Oligocene volcanic ashes of east and central Texas: Geological Society of America Bulletin, v. 127, p. 770–780, doi:10.1130/B31146.1.

Hiess, J., Nutman, A.P., Bennett, V.C., and Holden, P., 2008, Ti-in-zircon thermometry applied to contrasting Archean metamorphic and igneous systems: Chemical Geology, v. 247, p. 323–338, doi:10.1016/j.chemgeo.2007.10.012.

Hiess, J., Yi, K., Woodhead, J., Ireland, T., and Rattenbury, M., 2015, Gondwana margin evolution from zircon REE, O and Hf signatures of Western Province gneisses, Zealandia, *in* Roberts, N.M.W., et al., eds., Continent formation through time: Geological Society of London Special Publication 389, p. 323–353, doi:10.1144/SP389.10.

Hinkley, T.K., Smith, K.S., Taggart, J.E., Jr., and Brown, J.T., 1980, Chemical and mineralogical aspects of the observed fractionation of ash from the May 18, 1980 eruption of Mount St. Helens: U.S. Geological Survey Professional Paper 1397-A, 73 p.

Jarvis, K.E., 1988, Inductively coupled plasma mass spectrometry; a new technique for the rapid or ultra-trace level determination of the rare-earth elements in geological materials: Chemical Geology, v. 68, p. 31–39, doi:10.1016/0009-2541(88)90084-8.

Jenner, G.A., Longerich, H.P., Jackson, S.E., and Fryer, B.J., 1990, ICP-MS—A powerful tool for high-precision trace-element analysis in Earth sciences: Evidence from analysis of selected U.S.G.S. reference samples: Chemical Geology, v. 83, p. 133–148, doi:10.1016/0009-2541(90)90145-W.

Johnson, D.M., Hooper, P.R., and Conrey, R.M., 1999, XRF analysis of rocks and minerals for major and trace elements on a single low dilution Li-tetraborate fused bead: Advances in X-ray Analysis, v. 41, p. 843–867.

Jourdan, F., Féraud, G., Bertrand, H., Kampunzu, A.B., Tshoso, G., Watkeys, M.K., and Le Gall, B., 2005, Karoo large igneous province: Brevity, origin, and relation to mass extinction questioned by new $^{40}Ar/^{39}Ar$ age data: Geology, v. 33, p. 745–748, doi:10.1130/G21632.1.

Kelley, K.A., and Cottrell, E., 2009, Water and the oxidation state of subduction zone magmas: Science, v. 325, p. 605–607, doi:10.1126/science.1174156.

Kirkland, C.L., Smithies, R.H., Taylor, R.J.M., Evans, N., and McDonald, B., 2015, Zircon Th/U ratios in magmatic environs: Lithos, v. 212–215, p. 397–414, doi:10.1016/j.lithos.2014.11.021.

Kleiman, L.E., and Japas, M.S., 2009, The Choiyoi volcanic province at 34°S–36°S (San Rafael, Medoza, Argentina): Implications for the late Palaeozoic evolution of the southwestern margin of Gondwana: Tectonophysics, v. 473, p. 283–299, doi:10.1016/j.tecto.2009.02.046.

Kleiman, L.E., and Salvarredi, J.A., 2001, Petrología, geoquímica, e implicancias tectónicas del volcanismo triásico (Formación Puesto Viejo), Bloque de San Rafael, Mendoza: Revista de la Asociación Geológica Argentina, v. 56, p. 559–570.

Klemetti, E.W., and Clynne, M.A., 2014, Localized rejuvenation of a crystal mush recorded in zircon temporal and compositional variation at the Lassen Volcanic Center, northern California, Plos ONE, v. 9, e113157, 22 p., doi:10.1371/journal.pone.0113157.

Klemetti, E.W., Lackey, J.S., and Starnes, J., 2014, Magmatic lulls in the Sierra Nevada captured in zircon from rhyolite of the Mineral King pendant, California: Geosphere, v. 10, p. 66–79, doi:10.1130/GES00920.1.

Kohn, M.J., and Corrie, S.L., 2011, Preserved Zr-temperatures and U-Pb ages in high-grade metamorphic titanite; evidence for a static hot channel in the Himalayan orogen: Earth and Planetary Science Letters, v. 311, p. 136–143, doi:10.1016/j.epsl.2011.09.008.

Kylander-Clark, A.R.C., Hacker, B.R., and Cottle, J.M., 2013, Laser-ablation split-stream ICP petrochronology: Chemical Geology, v. 345, p. 99–112, doi:10.1016/j.chemgeo.2013.02.019.

Lanci, L., Tohver, E., Wilson, A., and Flint, S., 2013, Upper Permian magnetic stratigraphy of the lower Beaufort Group, Karoo Basin: Earth and Planetary Science Letters, v. 375, p. 123–134, doi:10.1016/j.epsl.2013.05.017.

Lawver, L.A., Gahagan, L.M., and Coffin, M.F., 1992, The development of paleoseaways around Antarctica: Antarctic Research Series, v. 56, p. 7–30, doi:10.1029/AR056p0007.

Li, X.-H., Liang, X., Sun, M., Liu, Y., and Tu, X., 2000, Geochronology and geochemistry of single-grain zircons; simultaneous in-situ analysis of U-Pb age and trace elements by LAM-ICP-MS: European Journal of Mineralogy, v. 12, p. 1015–1024, doi:10.1127/0935-1221/2000/0012-1015.

Lichte, F.E., Meier, A.L., and Crock, J.G., 1987, Determination of the rare-earth elements in geological materials by inductively coupled plasma mass spectrometry: Analytical Chemistry, v. 59, p. 1150–1157, doi:10.1021/ac00135a018.

Longerich, H.P., Jenner, G.A., Fryer, B.J., and Jackson, S.E., 1990, Inductively coupled plasma-mass spectrometric analysis of geological samples: A critical evaluation based on case studies: Chemical Geology, v. 83, p. 105–118, doi:10.1016/0009-2541(90)90143-U.

López-Gamundi, O.R., and Rossello, E.A., 1998, Basin fill evolution and paleotectonic patterns along the Samfrau geosyncline: The Sauce Grande basin–Ventana foldbelt (Argentina) and

Karoo basin–Cape foldbelt (South Africa) revisited: Geologische Rundschau, v. 86, p. 819–834, doi:10.1007/s005310050179.
Ludwig, K.R., 2009, Squid 2, A user's manual: Berkeley Geochronology Center Special Publication 5, 110 p.
Ludwig, K.R., 2012, Isoplot 3.75, a geochronological toolkit for Excel: Berkeley Geochronology Center Special Publication 5, 75 p.
Mantle, G.W., and Collins, W.J., 2008, Quantifying crustal thickness variations in evolving orogens: Correlation between arc basalt composition and Moho depth: Geology, v. 36, p. 87–90, doi:10.1130/G24095A.1.
McClelland, W.C., Gilotti, J.A., Mazdab, F.K., and Wooden, J.L., 2009, Trace-element record in zircons during exhumation from UHP conditions, north-east Greenland Caledonides: European Journal of Mineralogy, v. 21, p. 1135–1148, doi:10.1127/0935-1221/2009/0021-2000.
McKay, M.P., Weislogel, A.L., Fildani, A., Brunt, R.L., Hodgson, D.M., and Flint, S.S., 2015, U-Pb zircon tuff geochronology from the Karoo Basin, South Africa: Implications of zircon recycling on stratigraphic age controls: International Geology Review, v. 57, p. 393–410, doi:10.1080/00206814.2015.1008592.
McLachlan, I.R., and Jonker, J.P., 1990, Tuff beds in the northwestern part of the Karoo Basin: South African Journal of Geology, v. 92, p. 329–338.
Millar, I.L., Pankhurst, R.J., and Fanning, C.M., 2002, Basement chronology of the Antarctic Peninsula: Recurrent magmatism and anataxis in the Palaeozoic Gondwana margin: Journal of the Geological Society [London], v. 159, p. 145–157, doi:10.1144/0016-764901-020.
Moyen, J., 2009, High Sr/Y and La/Yb ratios: the meaning of the "adakitic signature": Lithos, v. 112, p. 556–574, doi:10.1016/j.lithos.2009.04.001.
Ottone, E.G., Monti, M., Marsicano, C.A., de la Fuente, M.S., Naipauer, M., Armstrong, R., and Mancuso, A.C., 2014, A new Late Triassic age for the Puesto Viejo Group (San Rafael depocenter, Argentina): SHRIMP U-Pb zircon dating and biostratigraphic correlations across southern Gondwana: Journal of South American Earth Sciences, v. 56, p. 186–199, doi:10.1016/j.jsames.2014.08.008.
Pankhurst, R.J., Rapela, C.W., Fanning, C.M., and Márquez, M., 2006, Gondwanide continental collusion and the origin of Patagonia: Earth-Science Reviews, v. 76, p. 235–257, doi:10.1016/j.earscirev.2006.02.001.
Pearce, J.A., Harris, N.B.W., and Tindle, A.G., 1984, Trace element discrimination diagrams for the tectonic interpretation of granitic rocks: Journal of Petrology, v. 25, p. 956–983, doi:10.1093/petrology/25.4.956.
Perkins, M.E., and Nash, B.P., 2002, Explosive silicic volcanism of the Yellowstone hotspot: The ash fall tuff record: Geological Society of America Bulletin, v. 114, p. 367–381, doi:10.1130/0016-7606(2002)114<0367:ESVOTY>2.0.CO;2.
Ramos, V.A., and Kay, S.M., 1991, Triassic rifting and associated basalts in the Cuyo basin, central Argentina, *in* Harmon, R.S., and Rapela, C.W., eds., Andean magmatism and its tectonic setting: Geological Society of America Special Paper 265, p. 79–92, doi:10.1130/SPE265-p79.
Riley, T.R., Flowerdew, M.J., Whitehouse, M.J., 2012, U-Pb ion-microprobe zircon geochronology from the basement inliers of eastern Graham Land, Antarctic Peninsula: Journal of the Geological Society [London], v. 169, p. 381–393, doi:10.1144/0016-76492011-142.
Rocha-Campos, A.C., Basei, M.A.S., Nutman, A.P., and Dos Santos, P.R., 2006, SHRIMP U-Pb zircon geochronological calibration of the late Paleozoic supersequence, Paraná Basin, Brazil: V South American Symposium on Isotope Geology, Punta del Este, Short Papers, p. 298–301.
Rocha-Campos, A.C., Basei, M.A.S., Nutman, A.P., Kleiman, L.E., Varela, R., Llambías, E., Canile, F.M., da Rosa, O. de C.R., 2011, 30 million years of Permian volcanism recorded in the Choiyoi igneous province (W Argentina) and their source for younger ash fall deposits in the Paraná Basin: SHRIMP U-Pb zircon geochronology evidence: Gondwana Research, v. 19, p. 509–523, doi:10.1016/j.gr.2010.07.003.
Rubatto, D., 2002, Zircon trace element geochemistry: partitioning with garnet and the link between U-Pb ages and metamorphism: Chemical Geology, v. 184, p. 123–138, doi:10.1016/S0009-2541(01)00355-2.
Rubatto, D., and Hermann, J., 2007, Experimental zircon/melt and zircon/garnet trace element partitioning and implications for the geochronology of crustal rocks: Chemical Geology, v. 241, p. 38–61, doi:10.1016/j.chemgeo.2007.01.027.
Rubidge, B.S., Erwin, D.H., Ramezani, J., Bowring, S.A., and de Klerk, W.J., 2013, High-precision temporal calibration of Late Permian vertebrate biostratigraphy: U-Pb zircon constraints from the Karoo Supergroup, South Africa: Geology, v. 41, p. 363–366, doi:10.1130/G33622.1
Rudnick, R.L., 1992, Restites, Eu anomalies, and the lower continental crust: Geochimica et Cosmochimica Acta, v. 56, p. 963–970, doi:10.1016/0016-7037(92)90040-P.
Schmitt, A.K., Wetzel, F., Cooper, K.M., Zou, H., and Wörner, G., 2010, Magmatic longevity of Laacher See volcano (Eifel, Germany) indicated by U-Th dating of intrusive carbonatites: Journal of Petrology, v. 51, p. 1053–1085, doi:10.1093/petrology/egq011.
Schoene, B., Schlategger, U., Brack, P., Latkoczy, C., Stracke, A., and Günther, D., 2012, Rates of magma differentiation and emplacement in a ballooning pluton recorded by U-Pb TIMS-TEA, Adamello batholith, Italy: Earth and Planetary Science Letters, v. 355–356, p. 162–173, doi:10.1016/j.epsl.2012.08.019.
Sircombe, K.N., and Stern, R.A., 2002, An investigation of artificial biasing in detrital zircon U-Pb geochronology due to magnetic separation in sample preparation: Geochimica et Cosmochimica Acta, v. 66, p. 2379–2397, doi:10.1016/S0016-7037(02)00839-6.
Spalletti, L.A., Fanning, C.M., and Rapela, C.W., 2008, Dating the Triassic continental rift in the southern Andres: the Potrerillos Formation, Cuyo Basin, Argentina: Geologica Acta, v. 6, p. 267–283.
Stacey, J., and Kramers, J.D., 1975, Approximation of terrestrial lead isotope evolution by a two-stage model: Earth and Planetary Science Letters, v. 26, p. 207–221, doi:10.1016/0012-821X(75)90088-6.
Taylor, H.E., and Lichte, F.E., 1980, Chemical composition of Mount St. Helens volcanic ash: Geophysical Research Letters, v. 7, p. 949–952, doi:10.1029/GL007i011p00949.
Tomlinson, E.L., Albert, P.G., Wulf, S., Brown, R.J., Smith, V.C., Keller, J., Orsi, F., Bourne, A.J., and Menzies, M., 2014, Age and geochemistry of tephra layers from Ischia, Italy: Constraints from proximal-distal correlations with Lago Grande di Monticchio: Journal of Volcanology and Geothermal Research, v. 287, p. 22–39, doi:10.1016/j.jvolgeores.2014.09.006.
Veevers, J.J., Cole, D.I., and Cowan, E.J., 1994, Southern African: Karoo basin and Cape fold belt, *in* Veevers, J.J., and Powell, C.M., eds., Permian-Triassic Pangean basins and foldbelts along the Panthalassan margin of Gondwanaland: Geological Society of America Memoir 184, p. 223–279, doi:10.1130/MEM184-p223.
Watson, E.B., and Harrison, T.M., 1983, Zircon saturation revisited: Temperature and composition effects in a variety of crustal magma types: Earth and Planetary Science Letters, v. 64, p. 295–304, doi:10.1016/0012-821X(83)90211-X.
Watson, E.B., and Harrison, T.M., 2005, Zircon thermometer reveals minimum melting conditions on earliest Earth: Science, v. 308, p. 841–844, doi:10.1126/science.1110873.
Watson, E.B., Wark, D.A., and Thomas, J.B., 2006, Crystallization thermometers for zircon and rutile: Contributions to Mineralogy and Petrology, v. 151, p. 413–433, doi:10.1007/s00410-006-0068-5.
Weislogel, A., Brunt, R.L., Flint, S., Fildani, A., and Rothfuss, J., 2011, Constraints on deepwater sedimentation in the Karoo Basin, South Africa, from U-Pb Geochronology of the ash interbeds: AAPG Search and Discover, Article #90124.
Winchester, J.A., and Floyd, P.A., 1977, Geochemical discrimination of different magma series and their differentiation products using immobile elements: Chemical Geology, v. 20, p. 325–343, doi:10.1016/0009-2541(77)90057-2.